arrays at positions that matched their original positions at the entrance aperture of the Bowen slicer. These arrays were the sought-for monochromatic images of the planet. The image slicer used for this work had a 5.2 × 5.2 arc sec aperture. The slicer used before August 1989 provided a 5 × 12 array of 60 data points, each of which represented an angular area of 1.04 × 0.43 arc sec. The slicer used during August yielded 8 usable slices and an 8 × 12 array of 96 data points, each of which represented an angular area of 0.52 × 0.43 arc sec. For convenience in working with the data, we resampled the arrays to provide either a 12 × 12 or a 10 × 12 array (depending on which of the two slicers was used) of data points, each one corresponding to an angular area of 0.43 × 0.43 arc sec.
14. B. Hapke, *J. Geophys. Res.* **86**, 3039 (1981).
15. J. Veverka *et al.*, in *Mercury*, F. Vilas, C. R. Chapman, M. S. Matthews, Eds. (Univ. of Arizona Press, Tucson, 1988), p. 37.
16. The image stabilizer used for these observations was a DTI-221 high-speed video guider (Digital Television Imagery) and is a fourth generation of the "leaky memory guiders" used at Kitt Peak National Observatory.
17. D. N. Baker, J. E. Borovsky, J. O. Burns, G. R. Gisler, M. Zerlik, *J. Geophys. Res.* **92**, 4707 (1987).
18. W. H. Ip, *Geophys. Res. Lett.* **14**, 1191 (1988).
19. Both authors are visiting astronomers at the National Solar Observatory, operated by the Association of Universities for Research in Astronomy, Inc., under contract with the National Science Foundation. A.E.P. was supported by the National Aeronautics and Space Administration (NASA) Planetary Astronomy Program. T.H.M. was supported by the National Research Council. The authors acknowledge helpful comments from the referees, R. M. Killen, M. McGrath, J. Rahe, and H. Zook.

21 November 1989; accepted 7 March 1990

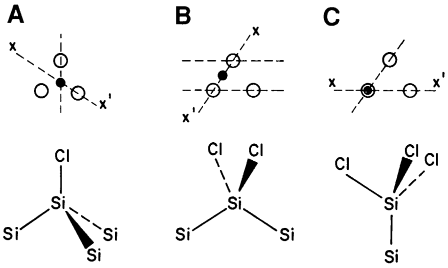

Fig. 1. Schematic showing the three possible reaction products. (**A**) SiCl, (**B**) $SiCl_2$, and (**C**) $SiCl_3$. The (111) surface is defined by the three rest atoms (O). The dashed lines correspond to the lines shown in Figs. 2 and 3. The top view (upper panel) shows the positions of all three rest atoms and the Si adatom, whereas the side view (lower panel) shows the Cl atoms and only the rest atoms that remain bonded to the adatom.

Identification of the Products from the Reaction of Chlorine with the Silicon(111)-(7×7) Surface

JOHN J. BOLAND AND J. S. VILLARRUBIA*

The various products from the reaction of chlorine (Cl) with the adatom layer of the Si(111)-(7×7) surface have been identified with scanning tunneling microscopy (STM). Initially, a single Cl atom reacts with the adatom dangling bond. At higher surface coverage, additional Cl atoms insert themselves into the Si–Si backbonds between the adatom and rest-atom layers, producing adatoms that have reacted with two or three Cl atoms. These products are characterized by different registries with respect to the underlying rest layer and appear in STM images as adatoms of different sizes, consistent with the breaking of Si–Si backbonds and the formation of new Si–Cl bonds.

SCANNING TUNNELING MICROSCOPY has developed into a powerful tool for the study of surfaces. The strength of STM lies in its ability to resolve, both in energy and real space, the electronic states of the surface within some energy window about the Fermi level E_f (*1*). Clean and adsorbate covered surfaces, in addition to thin overlayers, have been studied. Simple nondissociative adsorbates are identified on the basis of their known structural and electronic properties (*2*). Frequently, however, surface-adsorbate interactions involve significant bond making and breaking that result in the formation of a variety of different surface species. Although the presence of such species may be inferred spectroscopically, the ability of STM to identify the different products from a surface chemical reaction has yet to be established.

In this report we show that it is possible to distinguish between the various products from the reaction of Cl with the adatom layer of the Si(111)-(7×7) surface. These products, which correspond to three different Si adatom oxidation states, are characterized by different registries with respect to the underlying rest layer to which they are bonded. Furthermore, the different products are observed as adatoms of different sizes which is shown to be consistent with the breaking of successive Si–Si backbonds and the formation of new Si–Cl bonds.

The STM used in this work is similar to that described by Demuth *et al.* (*3*) and was mounted in an ion-pumped vacuum chamber with a base pressure of $\sim 1 \times 10^{-10}$ torr. The (7×7) surface was generated by heating a phosphorus-doped (1 ohm-cm) Si(111) wafer to 1050°C for 30 s. The Cl source was a AgCl electrochemical cell (*4*). The data shown consist of standard STM topographs in which the tunneling bias refers to the voltage on the sample.

The Si(111)-(7×7) surface adatom layer consists of triangular subunits that each contain six Si adatoms arranged locally in a (2×2) structure (*5*). These adatoms lie along or parallel to lines that bisect the triangular subunits of the cell. Each Si atom in the adatom layer has three backbonds to the Si atoms in the rest layer beneath and is situated in the threefold hollow formed by these rest atoms. The remaining Si adatom bonding orbital constitutes the adatom dangling bond (db), which point into the vacuum. In the present context the term adatom refers to the Si atoms in the adatom layer and not to the Cl atoms that subsequently react with this layer.

In an earlier report (*6*) we showed that at low surface coverages the Cl primarily interacts with the adatom db state and results in it occupying a site directly above the Si adatom. Therefore, adatoms that have reacted with a single Cl atom do not shift their positions from that of the unreacted surface and are situated in threefold hollow sites (Fig. 1A). As the coverage increases the Cl penetrates the relatively open adatom structure and inserts itself in one of the three backbonds between the adatom and the atoms in the rest layer beneath. Under saturation conditions, the rest atom db produced by this bond breaking is tied up by Cl. The reaction of the adatom with this additional Cl atom causes it to flip up out of the threefold hollow site and into a position where it is equidistant between the two remaining rest atoms to which it is bonded, lying along the line connecting these atoms in a bridge-bonding configuration (Fig. 1B). The reaction of a further Cl atom results in the breaking of one of these two backbonds, with the adatom now occupying an atop site directly above the remaining rest atom to which it is bonded (Fig. 1C).

X-ray photoelectron spectroscopy shows that all three adatom species are present after a room-temperature saturation dose of the surface (*7*). However, after a 400°C anneal the monochloro species predominates (*7*). Recently, we showed that this annealing process is associated with the transformation of an initially disordered (7×7) adatom structure to one in which the adatoms are stripped from the surface and accumulated

IBM Research Division, Thomas J. Watson Research Center, Yorktown Heights, NY 10598.

*Present address: National Institute of Standards and Technology, Gaithersburg, MD 20899.

in islands (*6, 8*). At higher temperatures these adatom islands fall apart and the adatoms are redistributed over the surface. As a result there is a limited temperature range over which the majority of the adatoms are in the form of islands, making registry measurements possible, and where the di- and trichloro species remain stable.

Rendered STM topographs of the three surface species (Fig. 2) were acquired following a saturation Cl dose and a 3-min anneal at approximately 400°C. The surface, which then consisted of isolated adatoms and adatom islands (*6, 8*), was subsequently redosed with Cl to convert some of the SiCl adatom species into the $SiCl_2$ and $SiCl_3$ forms. Even prior to the second dose the surface contained some of the latter species.

The saturation Cl dose tied up all the surface dbs and current-voltage (*I-V*) curves measured at positions above the adatom species and the adjacent rest layer showed the presence of a surface band gap. There were no striking differences between *I-V* curves recorded over the different adatom species. However as suggested by Fig. 1, the extent of the reaction at each of these sites may be determined by an accurate placement of the adatom's position on the surface. To aid in this determination, lines have been ruled along rows of atoms in Fig. 2. The corner adatom in Fig. 2A is seen to be positioned along a line that runs parallel to a bisector of the triangular subunit. The spacing between these lines corresponds to one half the interadatom spacing along the $\langle 0\bar{1}1 \rangle$ direction of the (7×7) cell (*5*). The adatom is located at the intersection between this line and the bisector (X-X′) from another side of the triangle. This position corresponds to the normal threefold hollow adatom bonding site of the unreacted surface (*5*), indicating that this adatom is a SiCl species. Note that the rest atoms that comprise the threefold hollow are obscured by the adatom. The adatom in Fig. 2B, however, is situated between two rows of atoms in one direction in addition to being along the row of atoms labeled X-X′. This corresponds to the bridge-bonding configuration shown in Fig. 1B, and we assign this adatom to be a $SiCl_2$ species. The remaining adatom shown in Fig. 2C is positioned along rows of atoms in both directions such that it is located in an atop site directly above a single rest atom and hence corresponds to the $SiCl_3$ species described in Fig. 1C.

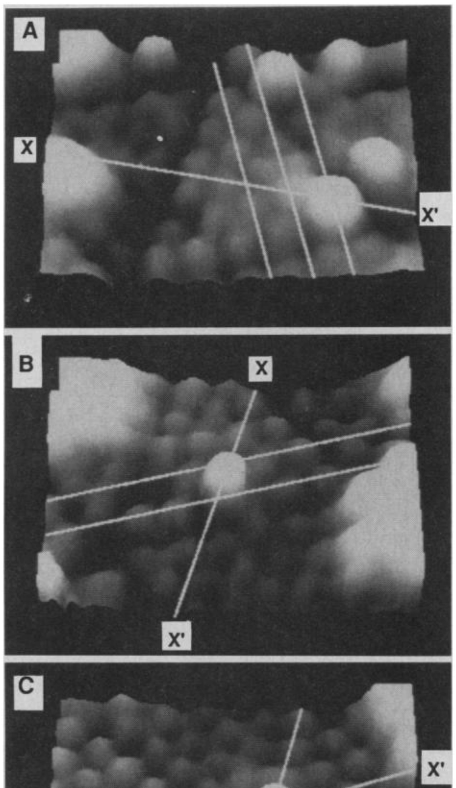

Fig. 2. Three-dimensional rendering of STM topographs recorded at +2 V showing (**A**) SiCl, (**B**) $SiCl_2$, and (**C**) $SiCl_3$ species. The area shown is 40 Å by 29 Å. Lines have been ruled along rows of atoms to aid in the location of the adatoms on the surface (see text). Note that rendering necessarily redistributes the adatom intensities in the tilt direction.

Cross sections along the lines labeled X-X′ in these topographs are shown in Fig. 3. The upward pointing arrows indicate the positions of the rest atoms along the individual sections. Note that the spacing between rest atoms in the direction X-X′ chosen in Fig. 3A is $\sqrt{3}$ times larger than that in Fig. 3, B and C. The adatom in Fig. 3A is located two thirds of the way between the rest atoms in this cross section, a position consistent with its location in the threefold hollow at the corner of the cell (*5*). The adatoms in Fig. 3, B and C, are positioned between and on top of rest atoms in their respective cross sections consistent with their identification as $SiCl_2$ and $SiCl_3$ species.

A striking feature of the images shown in Fig. 2 is that the three types of adatoms look very different. This is even more apparent from the cross sections of Fig. 3. The shoulders on the adatoms in Fig. 3, A and C, are due to overlapping intensity from a neighboring rest atom. The individual peaks were resolved by fitting a sum of gaussians to the data and are shown as dashed curves in Fig. 3. All three types of adatoms could be fitted with gaussians of approximately the same width. The different appearances of these adatoms is then due to their varying heights above the rest layer. This height, denoted by Δh in Fig. 3, was determined by measuring the adatom peak height with respect to the average height of the rest layer. Based on these results and the assignments discussed earlier, the greater the number of Cl atoms bonded to a Si adatom, the smaller the height of the surface protrusion associated with that adatom. This effect is not due to local differences in the height of the tunneling barrier arising from variations in the surface dipole moment between the adatom sites. In fact, from calculations based on the polarity and directionality of the Si–Cl bonds we find that the barrier should be largest for the species containing the fewest Cl atoms.

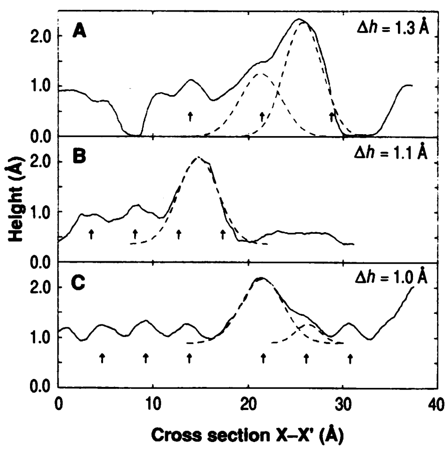

Fig. 3. (**A** through **C**) Cross sections X-X′ derived from the topographs in Fig. 2. The dashed curves are the gaussian components of the adatom peaks. The arrows indicate the positions of the rest atoms.

This size difference is due in part to the breaking of Si–Si backbonds as additional Si–Cl bonds are formed. These backbond states are located 1.5 eV above E_f and are known to contribute to the tunneling current observed over adatom sites (*9*). However, earlier we showed that tunneling over these reacted adatom sites also occurs into the tail of an empty Cl-derived σ^* state that is broadened because of hybridization with the bulk (*6*). This state is calculated to be ~4 eV above E_f but disperses strongly over the Brillouin zone (*10*). Ab initio molecular orbital calculations of Cl on Si clusters and a series of related chlorosilanes, each designed to model the structures of the different adatom species, show that the strength of the Si-Cl (σ-σ^*) energy splitting increases with the number of Cl atoms in the cluster or molecule. Furthermore, the energy of the σ^* state is progressively shifted to higher values, with a 0.6-eV energy difference between the states associated with the SiCl-and $SiCl_3$-like species (*11*). This enhanced splitting is consistent with the greater orbital overlap and bond strength of Si–Cl bonds compared to Si–Si bonds. A similar trend has been reported for the analogous hydride species present on both the hydrogenated Si(111)-(7×7) and amorphous Si surfaces (*12, 13*). Based on these results we suggest that the intensity of both the backbond state and the tail of the σ^* state that extends into the tunneling energy window depends on the adatom species from which they are derived, both being more pronounced for those that contain fewer Cl atoms. This behavior is directly reflected in the topographs of Fig. 2, where in order to maintain the required stabilization current the tip-to-surface distance must decrease as the number of Cl atoms bonded to the adatom increases.

Although reacted and unreacted db sites can be readily distinguished with the use of *I-V* curves (*6, 9*), we were unable to distinguish between the different chlorinated adatoms with this method. The differences in the latter case are subtle and involve changes in the shape of the background. The problem arises from the presence of bulk states that dominate the *I-V* curves and mix with and broaden the states of interest. Furthermore, *I-V* curves recorded at a given site on the surface are normalized to the current at that site (*1*), making it difficult to compare the shape and size of the backgrounds at different surface sites. Despite this, the different products known to exist on this surface can be distinguished on the basis of their registry and appear as adatoms of different sizes consistent with the number of Si–Si and Si–Cl bonds they contain.

REFERENCES AND NOTES

1. R. M. Feenstra, J. A. Stroscio, A. P. Fein, *Surf. Sci.* **181**, 295 (1986).
2. See, for example, H. Ohani, R. J. Wilson, S. Chang, C. M. Mate, *Phys. Rev. Lett.* **60**, 2398 (1988).
3. J. E. Demuth, R. J. Hamers, R. M. Tromp, M. E. Welland, *J. Vac. Sci. Technol. A* **4**, 1320 (1986).
4. R. D. Schnell, D. Rieger, A. Bogen, K. Wandelt, W. Steinmann, *Solid State Commun.* **53**, 205 (1985).
5. K. Takayanagi, Y. Tanishiro, S. Takahashi, M. Takahashi, *Surf. Sci.* **164**, 367 (1985).
6. J. J. Boland and J. S. Villarrubia, *Phys. Rev. B*, in press.
7. R. D. Schnell *et al.*, *ibid.* **32**, 8057 (1985).
8. J. S. Villarrubia and J. J. Boland, *Phys. Rev. Lett.* **63**, 306 (1989).
9. R. Wolkow and Ph. Avouris, *ibid.* **60**, 1049 (1988).
10. M. Schlüter and M. L. Cohen, *Phys. Rev. B* **17**, 716 (1978).
11. J. J. Boland and A. Rossi, unpublished results.
12. K. M. Ho, M. L. Cohen, M. Schlüter, *Phys. Rev. B* **15**, 3888 (1977).
13. B. von Roedern, L. Ley, M. Cardona, F. W. Smith, *Philos. Mag. B* **40**, 433 (1979).
14. We thank A Rossi for assistance with the calculations and J. Baker for use of his curve-fitting software.

24 January 1990; accepted 4 April 1990

Electro-Optical Evidence for the Chelate Effect at Semiconductor Surfaces

GEORGE C. LISENSKY,* RONA L. PENN, CATHERINE J. MURPHY, ARTHUR B. ELLIS*

Monoamines and diamines dissolved in cyclohexane solution reversibly enhance the band-edge photoluminescence (PL) intensity of immersed n-type cadmium sulfide (n-CdS) and n-type cadmium selenide (n-CdSe) substrates through adsorption. The magnitude of the PL increase is used to estimate amine-induced contractions in the semiconductor's depletion width, and the dependence of the PL intensity on amine concentration provides an estimate of the adduct formation constant. Two diamines, ethylenediamine and *o*-phenylenediamine, exhibit unusually low reductions in depletion width and substantially larger adduct equilibrium constants relative to the other amines studied, consistent with chelation to surface Cd^{2+} ions. These studies demonstrate that PL can be used as a contactless, in situ technique for characterizing the steric and electronic landscape of semiconductor surfaces and for correlating molecular and surface chemistry.

DESPITE THE IMPORTANCE OF SURface chemistry in semiconductor technology, its role in determining the electro-optical characteristics of semiconductor materials is not well understood (*1*). We have embarked on a program to characterize the surface chemistry of the II-VI semiconductors n-CdS and n-CdSe. Using the bandgap PL of the solid as a probe, we have characterized surface adduct formation with amines and butenes in the gas phase and with phosphines and lanthanide β-diketonate complexes in hydrocarbon solution (*2–5*).

In this report, we establish a link between classical coordination chemistry and surface chemistry by demonstrating chelation at the semiconductor-solution interface. The "chelate effect" refers to the enhanced stability of a coordination compound containing polydentate ligands relative to one with analogous monodentate ligands (*6*). An example of this effect is provided by the following comparison of displacement reactions in aqueous solution, where β_n is the overall formation constant for *n* ligands coordinated to the metal center, for which the bidentate amine has the larger formation constant (*7*):

$$Cd^{2+}(aq) + 4CH_3NH_2 \rightarrow Cd(CH_3NH_2)_4{}^{2+}, \log \beta_4 = 6.52 \qquad (1)$$

$$Cd^{2+}(aq) + 2H_2NCH_2CH_2NH_2 \rightarrow Cd(H_2NCH_2CH_2NH_2)_2{}^{2+}, \log \beta_2 = 10.6 \qquad (2)$$

That surface atoms could form part of a chelate ring with solution species has been hypothesized in several studies (*8*), including ones involving adsorption of dithiocarbamates from CH_3CN solution and of EDTA from aqueous solution onto CdS or CdSe (*9*). We provide evidence here from PL data that diamines can chelate to surface-lattice Cd^{2+} ions by adsorption from cyclohexane solution. Signatures of chelation are a smaller perturbation of the semiconductor's depletion [because of the low density of charge carriers in a semiconductor, the electric field, which results from charge trapped at the solid's surface, extends for some distance, known as the depletion width, into the solid (*10*)] and far larger adduct formation constants than are found for monoamines of comparable size. Our data also highlight the general use of PL as a contactless, in situ technique for characterizing semiconductor-derived interfaces.

We have focused on amines in this study because they form stable Cd^{2+} complexes (Eqs. 1 and 2). The diamines selected for study include ethylenediamine (en), *o*-phenylenediamine (opda), and 1,3-propanediamine (tn), which are almost always found

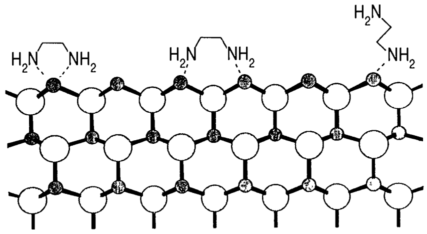

Fig. 1. Possible modes of en bonding are shown: from left to right, chelating, bridging, and monodentate bonding. The smaller circles represent Cd^{2+} sites; the larger circles represent S^{2-} or Se^{2-} sites. The 0001 face of CdS (or CdSe) is perpendicular to the plane of the figure, and the crystallographic *c* axis is indicated.

G. C. Lisensky and R. L. Penn, Department of Chemistry, Beloit College, Beloit, WI 53511.
C. J. Murphy and A. B. Ellis, Department of Chemistry, University of Wisconsin–Madison, Madison, WI 53706.

*To whom correspondence should be addressed.